

High-gain and high-speed wavefront shaping through scattering media

Received: 10 March 2022

Accepted: 12 December 2022

Published online: 23 January 2023

 Check for updates

Zhongtao Cheng , Chengmingyue Li, Anjul Khadria , Yide Zhang  & Lihong V. Wang  

Wavefront shaping (WFS) is emerging as a promising tool for controlling and focusing light in complex scattering media. The shaping system's speed, the energy gain of the corrected wavefronts and the control degrees of freedom are the most important metrics for WFS, especially for highly scattering and dynamic samples. Despite recent advances, current methods suffer from trade-offs that limit satisfactory performance to only one or two of these metrics. Here we report a WFS technique that simultaneously achieves high speed, high energy gain and high control degrees of freedom. By combining photorefractive crystal-based analogue optical phase conjugation and stimulated emission light amplification, our technique achieves an energy gain approaching unity; that is, more than three orders of magnitude larger than conventional analogue optical phase conjugation. The response time of $\sim 10 \mu\text{s}$ with about 10^6 control modes corresponds to an average mode time of about 0.01 ns per mode, which is more than 50 times quicker than some of the fastest WFS systems so far. We anticipate that this technique will be instrumental in overcoming the optical diffusion limit in photonics and translate WFS techniques to real-world applications.

In optically complex scattering media such as biological tissues, multimode fibres, white paper, clouds and fog, nanoscale refractive index inhomogeneities cause optical scattering that scrambles the wavefront of incident light. Such scattering has been a major obstacle to efficient light delivery and focusing, hindering optical imaging, manipulation, therapy and stimulation beyond the optical diffusion limit. The emerging wavefront shaping (WFS) technology shows promise for focusing light deeply through or into complex scattering media. By tailoring the optical wavefront incident on a scattering medium, WFS manipulates the interference of multiply scattered light to refocus it^{1,2}. To be a general tool for scattering suppression, an ideal WFS method would simultaneously have high system speed, high energy gains of the corrected wavefronts and high control degrees of freedom (DOF). To meet the speed requirement, WFS operations must be completed within the speckle correlation time, which is typically limited to 1 ms or less by physiological motion in living biological tissues. The energy gain is defined as the ratio of the energy of the corrected wavefront to that of the detected scattered wavefront, and it is related to the efficiency

of the wavefront modulation system³. A high energy gain ensures that the generated light focus has as much energy as possible to facilitate applications. An energy gain approaching or exceeding unity is generally highly desired. The control DOF of a WFS system determines the fineness of the wavefront modulation, thus determining the fidelity of optical focusing, which is particularly important for WFS in thick and highly scattering media.

Wavefront shaping technologies so far can be mainly divided into three categories: (1) feedback-based WFS^{1,4–11}, (2) transmission matrix inversion^{12–19} and (3) optical phase conjugation (OPC) or time reversal^{20–31}. The first two require thousands of measurements and wavefront updates to find a satisfactory modulation wavefront, resulting in a long runtime that scales linearly with the number of DOF; typical runtimes are on the level of a few seconds for methods using digital micromirror devices, or more for methods based on liquid crystal spatial light modulators (SLMs). Wavefront shaping in complex media with 2.4 ms latency was recently demonstrated by measuring the transmission matrix using a 1D microelectromechanical system-based phase

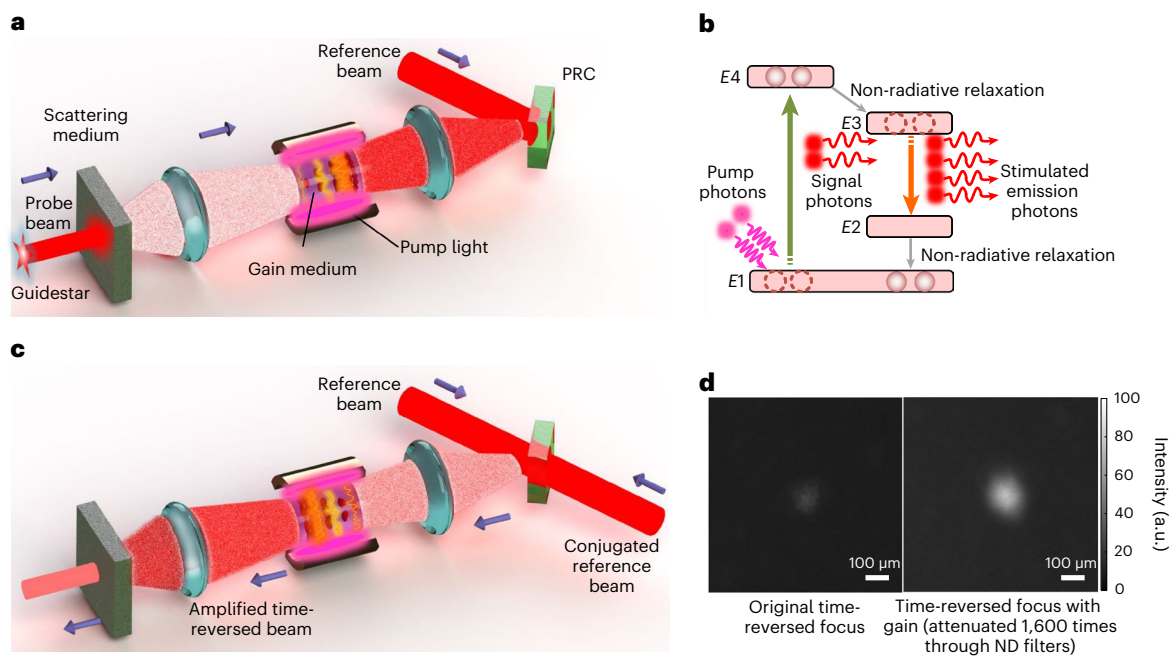


Fig. 1 | Principle of the HGHS-WFS. **a**, The probe beam scattered through the scattering medium is collected and directed to a gain module, which is composed of a gain medium and a pump source. The weak scattered photons are amplified in the gain module by stimulated emission light amplification and subsequently interfere with a reference beam to form a volume hologram inside of the PRC. **b**, Illustration of stimulated emission light amplification in a typical four-level gain medium, as used in our experiments; $E1$ – $E4$ denote the simplified four energy levels involved in the stimulated emission light amplification. **c**, Reading

the hologram inside of the PRC using a conjugated reference beam results in a weak time-reversed beam, which retraces its trajectory through the gain module and gains energy without change to its wavefront. After propagating through the scattering medium, the amplified time-reversed beam converges to the guidestar position. **d**, An example of the original time-reversed focus without the gain module, compared with the result of the proposed approach when focusing through a highly scattering optical diffuser. Note that the time-reversed focus with gain is attenuated $\sim 1,600$ times to avoid camera over-exposure.

modulator and a fast avalanche photodiode³²; however, this method works well only for WFS in thin scattering media due to the low control DOF of the 1D microelectromechanical systems. By contrast, OPC generates the optimal incident wavefront essentially instantaneously by recording the optical field of the scattered light and then playing back a time-reversed optical field to the scattering medium. The field recording and time reversal can be realized by combining a digital camera and an SLM, termed digital OPC (DOPC)^{3,20–28}, or by using a photorefractive crystal (PRC)^{29–31,33}, termed analogue OPC (AOPC). Most DOPC systems—limited by the frame rates of 2D cameras, the update rates of SLMs and data processing speeds—take more than tens of milliseconds to complete optical focusing. A DOPC system latency of about ~ 1 ms was recently reported for a frequency-encoded wavefront measurement approach using a single-pixel detector³⁴; however, the achievable control DOF ($\sim 1,000$)—determined by the achievable independent frequency components—was still the biggest limitation. Analogue OPC can complete the field recording and time reversal within several milliseconds to several seconds, depending on the material properties of the PRC employed and the illumination intensity. Unlike a digital SLM with discrete pixels of several micrometres, a PRC can be considered as an analogue SLM that has continuous modulation units (typical spatial resolution of $5,000$ – $10,000$ mm^{-1})³⁵. The accommodable control DOF of AOPC is therefore much higher than that of DOPC, which means that AOPC has the potential to realize high-fidelity optical focusing even through highly scattering samples; however, the largest disadvantage of AOPC is its low conjugation reflectivity, which is due to the weak nonlinear effect in the PRC and especially when the scattered beam incident on the crystal is weak. Consequently, the energy gain of the time-reversed beam is well below unity (typically 10^{-3} or less). The system speeds, control DOFs and energy gains in representative publications on WFS are compared in Supplementary Table 1 and discussed in Supplementary Note 1.

In this Article we report a WFS modality termed high-gain high-speed WFS (HGHS-WFS) that can simultaneously achieve high speed, high control DOF and high energy gain. We incorporate the concept of stimulated emission light amplification into an AOPC realization with a fast semiconductor PRC that has a submillisecond response time. The low conjugation reflectivity of the PRC is greatly compensated for by the gain from the stimulated emission, which results in WFS energy gains approaching unity in our experiments. Owing to the fast response of the PRC employed, as well as the amplified energy of the signal photons, we also demonstrate a system latency as fast as ~ 10 μs with a high control DOF of $\sim 10^6$. The average mode time (that is, the average operation time per mode) of the technique is more than 50-times lower than that of the fastest WFS system reported so far.

Results

Principle

The core idea of the proposed HGHS-WFS is combining the concept of stimulated emission light amplification with an AOPC-based WFS system that employs a semiconductor PRC with a submillisecond response time as the phase conjugation mirror. As schematically illustrated in Fig. 1a, a gain module—composed of a gain medium and a pump source—is inserted between the scattering medium and the PRC. A guidestar, which could be a collimated laser beam or other physical or virtual light source, transmits a probe beam through the scattering medium. A portion of the probe photons scattered through the medium are collected and directed via a collection lens into the gain module, where the weak scattered photons are amplified by stimulated emission light amplification. The original and amplified probe photons are subsequently directed to the PRC and interfere with a reference beam. Due to the photorefractive effect, information on the optical field incident on the PRC is encoded into a volume hologram inside of the PRC. In stimulated emission, the stimulated light wave will be coherent (in

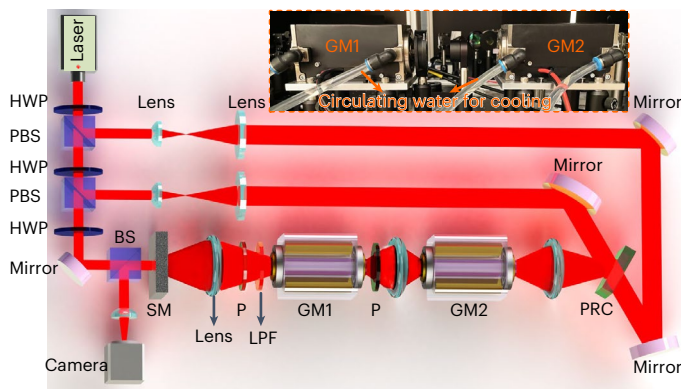


Fig. 2 | Schematic of the experimental set-up. The inset shows photos of the gain modules used in the experiments. BS, beam splitter; GM, gain module; HWP, half-wave plate; LPF, long-pass filter; P, polarizer; PBS, polarizing beam splitter; SM, scattering medium.

phase) with the incoming wave (Fig. 1b). The original photons and the amplified photons will thus have the same wavefront. In this way, we can increase the energy of the scattered field greatly with minimal change to its wavefront, which is important for the subsequent time reversal. The recorded hologram inside of the PRC is read out by a conjugated reference beam, resulting in a diffracted field that has a conjugated phase with the incident field on the PRC (Fig. 1c). The diffracted field retraces its trajectory through the gain module and gains energy. Similarly, as the light amplification does not affect the wavefront of the diffracted field, the conjugation characteristic of the amplified diffracted field is preserved. After propagating through the scattering medium, the amplified diffracted field converges to the guidestar position as a time-reversed wave. During all of these processes, stimulated emission light amplification plays an important role in providing gain to the scattered photons incident on the PRC and the conjugated photons reflected off the PRC, which greatly compensates for the low conjugation reflectivity of the PRC. Figure 1d, which demonstrates focusing through a highly scattering optical diffuser, presents an example result of the original time-reversed focus without the gain module, along with the result of the proposed approach.

As a proof-of-concept demonstration, we built the experimental system shown in Fig. 2 and detailed in the Methods. Briefly, a near-infrared laser (1,064 nm) is split into three beams that act as the probe, the reference and the conjugated reference beams, respectively. We employed two gain modules located in series in the path of the probe beam to provide sufficient gain to the system. Each gain module integrates an Nd:YAG rod as the gain medium and several laser diode arrays at 808 nm as pump sources. The pump sources are placed around the gain medium in a side-pump mode to produce a uniform pumping volume inside of the gain medium. In our configuration, the energy of the incident light can be increased ~50-fold after passing through each gain module (Supplementary Note 2). The PRC here is a GaAs semiconductor with a response time of less than 1 ms³⁶. In the proof-of-concept experiments, the guidestar can be considered as the incident collimated laser beam. The amplified time-reversed field therefore becomes a plane wave without scattering after propagating through the scattering medium. To validate the time-reversal performance, a beam splitter is inserted in front of the scattering medium to divert a copy of the time-reversed light to a camera.

Although it is straightforward to realize time reversal via separate hologram writing and reading modes, here we adopt a slightly different approach: the probe and reference beams are kept on when the conjugated reference beam is reading the hologram. Such a configuration is essentially a four-wave mixing mode³⁷. The advantages of such a time-reversal mode are twofold: first, the OPC reflectivity from the

four-wave mixing mode is much higher than that from the separate hologram writing and reading modes for the GaAs PRC, as experimentally demonstrated in Supplementary Note 3. Second, eliminating separate hologram writing and reading saves time, thus promoting the system speed. We note that for some PRCs with slow response speeds, lengthy writing is required to generate a strong hologram inside of the crystal. Separate hologram writing and reading modes may be a better choice in such a scenario. The proposed method can of course be directly applied to both time-reversal modes.

High-gain WFS through scattering media

We first demonstrate the HGHS-WFS using an optical diffuser with a diffusion angle of -10° (DG-120, Thorlabs) as the scattering medium. In this experiment, the power of the scattered probe beam collected on the PRC is ~ 1 mW. Figure 3a shows the original time-reversed focus without gain, whereas Fig. 3b shows the cross-section along the central row of the focus image. By contrast, Fig. 3c–f shows four typical images of the time-reversed foci through the scattering medium at 65%, 76%, 88% and 100% pump energy of the gain modules we used. Note that when capturing these four images, we placed an neutral density filter providing $\sim 1,600$ -fold attenuation in front of the camera to avoid it being damaged by the powerful intensity of the time-reversed light. For a good comparison to the results without gain, the attenuation-corrected profiles of the central cross-sections of Fig. 3c–f are presented in Fig. 3g. As can be seen, the peak intensity of the time-reversed focus increases to 1.024×10^5 from the original 19 without gain when the gain modules work at their maximum pump powers, an increase by a factor of $\sim 5,390$. The energy gain of the WFS system, which is defined as the ratio of the energy in the time-reversed light to that of the collected scattered light on the PRC, is only $(1.31 \pm 0.04) \times 10^{-4}$ for the original time reversal without gain; however, our HGHS-WFS increases the energy gain to 1.05 ± 0.02 , which is nearly four orders of magnitude better (Supplementary Note 4). The energy gains and the contrast-to-noise ratios (CNRs) of the time-reversed foci in Fig. 3c–f are presented in Fig. 3h. The CNR is defined as the ratio between the peak intensity of the time-reversed signal above the mean of the background, and the standard deviation of the background³⁸. Unlike digital WFS where the background around the optical focus appears as speckle patterns, in HGHS-WFS the background around the focus originates from the optical noise of the gain medium, which is optically incoherent and has a uniform intensity distribution. The CNR is a good gauge of the visibility of the focus pattern in our case as it evaluates both the peak intensity of the signal and the fluctuation of its background (rather than the background direct current value)³⁹. See Supplementary Note 5 for more illustrations about the CNR and the peak-to-background ratio (PBR) used in digital WFS. From Fig. 3h, the energy gain of the time-reversed focus increases with the increasing pump power of the gain modules, which is consistent with the results in Fig. 3g. We find that the fluctuation of the background from the gain medium increases faster at a higher pump power. An excessively high pump power may thus degrade the CNR, as can be seen in Fig. 3h. To augment the energy gain and the CNR simultaneously, it is better to raise the phase conjugation reflectivity of the PRC (see ‘Discussion’ section) while increasing the pump power.

To demonstrate the ability of the HGHS-WFS to focus through thicker scattering samples, we also performed experiments using different numbers of stacked optical diffusers and chicken breast tissue slices as samples. The results are presented in Supplementary Note 6.

High-speed WFS through dynamic scattering media

To demonstrate the practical system latency of the HGHS-WFS, we mounted a 4-mm-thick piece of chicken tissue on a motorized translation stage to produce a dynamic sample with a controllable speckle correlation time. Figure 4a shows several examples of the speckle correlation coefficient as a function of time when the sample was moved

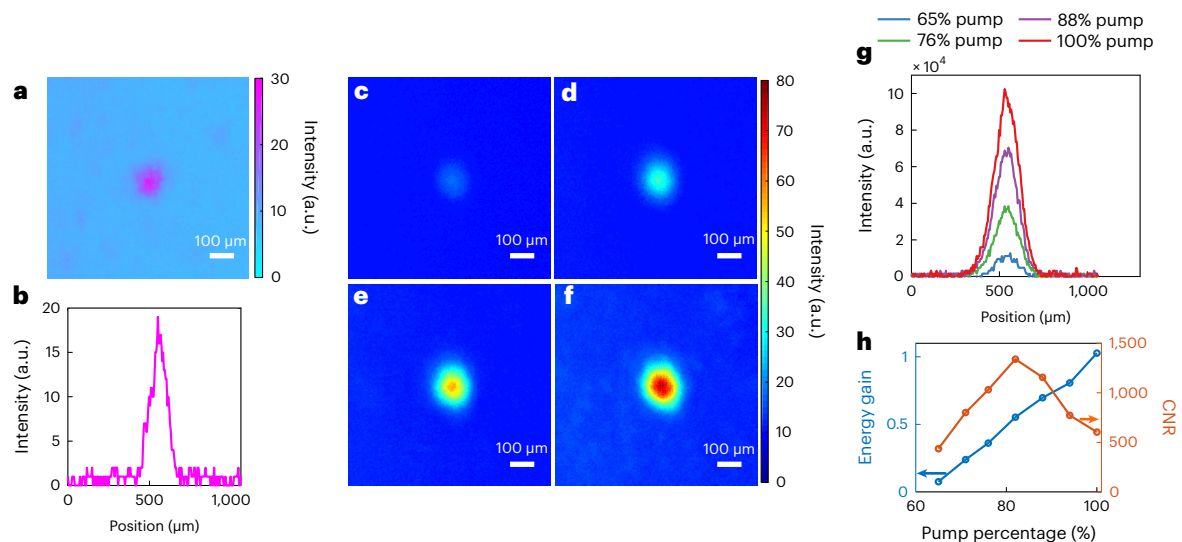


Fig. 3 | Experimental demonstrations of the HGHS-WFS at different pump powers of the gain modules. **a**, Original time-reversed focus without gain. **b**, Cross-section profile along the central row of the focus image in **a**. **c–f**, Four typical images of the obtained time-reversed foci through the scattering medium at 65% (**c**), 76% (**d**), 88% (**e**) and 100% (**f**) pump energy of the gain modules we

used. We placed a neutral density filter providing $-1,600$ -fold attenuation in front of the camera when capturing these four images. **g**, Attenuation-corrected profiles of the central cross-sections of **c–f**. **h**, Energy gains and CNRs of the time-reversed foci in **c–f**, as well as the foci at other pump energies whose images are not shown.

at different speeds (see Methods). The relationship between the speckle correlation time and the sample movement speed is shown in Fig. 4b, where the data are fitted to a theoretical model τ_c (ms) = d_b (μm)/ v (mm s^{-1}), in which $d_b = 5.37 \mu\text{m}$ is the fitted parameter from the experimental data. The value of τ_c at different speeds can be estimated from the fitted theoretical model, especially when the movement of the sample is so fast that the frame rate of the camera limits the direct measurement of τ_c . Figure 4c shows the time-reversed foci of the HGHS-WFS for four cases: (1) when the tissue was static ($\tau_c > 1$ s), and when it was moved at (2) $v = 300 \text{ mm s}^{-1}$ ($\tau_c = 17.9 \mu\text{s}$), (3) $v = 400 \text{ mm s}^{-1}$ ($\tau_c = 13.4 \mu\text{s}$), and (4) $v = 500 \text{ mm s}^{-1}$ ($\tau_c = 10.7 \mu\text{s}$). The peak intensities of the time-reversed foci obtained for the sample with different correlation times are shown in Fig. 4d. Our experiments here demonstrate that the performance of our HGHS-WFS does not obviously vary when the sample correlation time is larger than $15 \mu\text{s}$. The intensity of the time-reversed focus starts to decrease with faster speckle decorrelation, but we can still successfully realize time reversal, even when $\tau_c = 10.7 \mu\text{s}$, as shown in Fig. 4c.

In vivo optical focusing through a living-mouse ear

As a final demonstration, we applied HGHS-WFS for in vivo optical focusing through an area of a living mouse's ear with many blood vessels, where strong optical scattering, absorption, and fast speckle decorrelation co-exist. The scattering and absorption of the blood and other fluids in the living tissue meant that only about 1% of the incident optical power on the mouse ear could be collected to the PRC for time reversal. The speckle correlation time of the mouse ear was measured to be about 2 ms (see Methods), as shown in Fig. 5a. As the collected scattered light on the PRC was quite weak in this case, no time-reversed optical focus through the mouse ear could be observed for the conventional AOPC without gain (Fig. 5b). By contrast, as Fig. 5c shows, a bright optical focus was achieved with HGHS-WFS. The energy gain of the time-reversed focus is estimated to be 0.3 ± 0.01 .

Discussion

We presented an analogue time-reversal modality that enables WFS in scattering media with an energy gain approaching unity (that is, more than three orders of magnitude larger than conventional AOPC) while

exhibiting a response time of nearly $10 \mu\text{s}$. This WFS modality also maintains the intrinsically advantageous high control DOF found in conventional AOPC. For example, the speckle size on the PRC in the 4-mm-thick chicken tissue experiment was measured to be about $3.9 \mu\text{m}$; the practical number of the speckle modes controlled by the PRC was thus estimated to be $(A/d)^2 = (4 \times 10^3/3.9)^2 \approx 1.05 \times 10^6$, where $A = 4 \text{ mm}$ is the effective size of the PRC and d is the speckle size on the PRC; the average mode time is therefore about 0.01 ns per mode, which is more than 50-times lower than that in the fastest WFS system reported so far (0.6 ns per mode)¹¹.

Here we discuss the energy gain of the phase conjugation in HGHS-WFS, which can be improved further. In Supplementary Note 7 we show that it is the low phase conjugation reflectivity of the PRC that limits the energy gain of the time-reversed signal in our current configuration, mainly due to the low optical powers of the reference and conjugated reference beams available. Greater illumination powers on the PRC tend to produce a larger phase conjugation reflectivity and thus a larger energy gain. For example, if the powers of both the reference and conjugated reference beams can be increased to 1,000 mW (a tenfold increase with respect to the current powers), the energy gain could be improved by a factor of ~ 35 . Moreover, the phase conjugation reflectivity of the PRC can be largely augmented by applying an alternating current electric field to the crystal to enhance the space charge field within the crystal^{40,41}. For example, a 10 kV cm^{-1} electric field can improve the phase conjugation reflectivity by one order of magnitude relative to that without an external electric field. Furthermore, a higher energy gain could be obtained with higher pump powers for the gain modules (see Supplementary Note 7 for more detailed discussions). We also note that the sample should be properly tilted with respect to the optical axis of the gain crystal, which helps prevent stray light reflected by the sample from going back into the gain crystal and avoid possible parasitic oscillation largely, especially when the energy gain is much higher than unity.

Although increasing the illumination powers and applying an external high voltage to the PRC will help improve the intrinsic phase conjugation reflectivity of the PRC, the maximum value that can be achieved this way is only $\sim 10^{-3}$ (as calculated in Supplementary Note 7), which is determined by the material properties of the PRC.

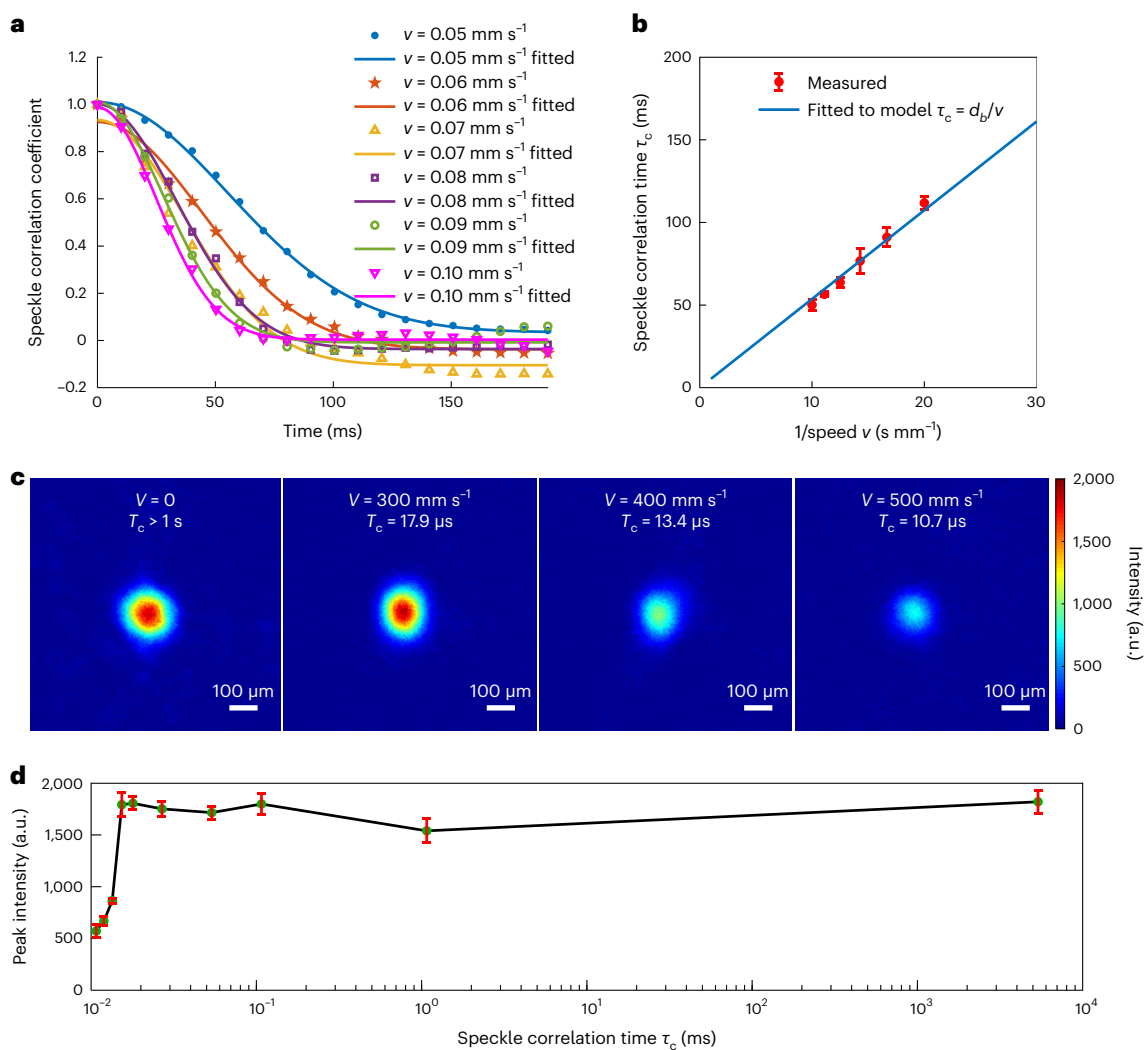


Fig. 4 | Focusing through fast dynamic scattering samples. a, Examples showing the speckle correlation coefficient as a function of time when the sample was moved at different speeds. **b**, Relationship between the speckle correlation time and the sample movement speed. The error bars show the s.d. of τ_c measured when light illuminates four different locations on the tissue. **c**, The

time-reversed foci of the HGHS-WFS when a 4-mm-thick piece of tissue was static ($\tau_c > 1 \text{ s}$), and when moved at $v = 300 \text{ mm s}^{-1}$ ($\tau_c = 17.9 \mu\text{s}$), $v = 400 \text{ mm s}^{-1}$ ($\tau_c = 13.4 \mu\text{s}$) and $v = 500 \text{ mm s}^{-1}$ ($\tau_c = 10.7 \mu\text{s}$). **d**, Peak intensities of the time-reversed foci through the sample with different correlation times. The error bars show the s.d. of the peak intensities of three time-reversed foci.

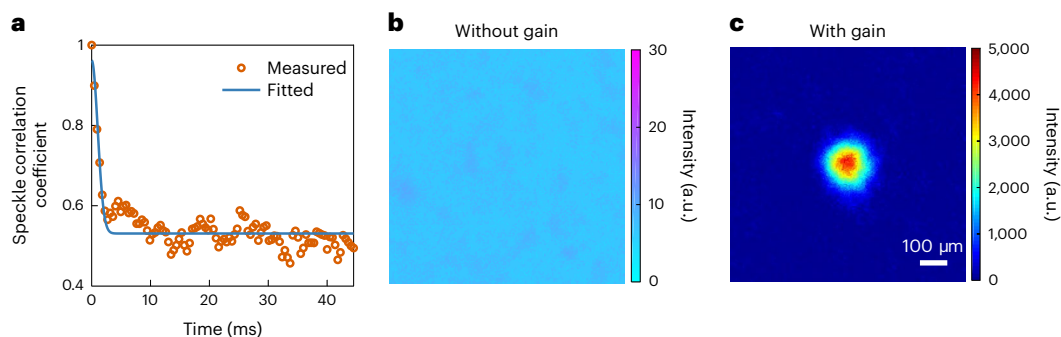


Fig. 5 | In vivo optical focusing through a living-mouse ear. a, Speckle correlation coefficient as a function of time for a living-mouse ear. **b, c**, Results of optical focusing through the mouse ear for conventional AOPC without gain (**b**) and for HGHS-WFS (**c**).

This result illustrates theoretically why the energy gain in conventional WFS based on PRCs is generally well below unity, as mentioned in the ‘Introduction’ section. The stimulated emission light amplification in our HGHS-WFS provides a practical solution for pushing the energy

gain of AOPC to close to unity or more. The ultrahigh system speed of the HGHS-WFS benefits from the intrinsic fast response of the GaAs crystal, the enhanced signal intensity on the PRC due to the energy amplification of the gain modules, and the four-wave mixing mode for

time reversal (Supplementary Notes 8 and 9). In some applications for which such a fast response is not required, we can also choose a slower but more efficient PRC as an alternative to the GaAs used here.

The proposed HGHS-WFS is a general time reversal system that can work independently for focusing through scattering media, as demonstrated here. It can also work with an internal guidestar, such as focused ultrasound or nanoparticles that generate a nonlinear second-harmonic signal, for focusing into scattering media^{21,30,42}. When working with an ultrasonic guidestar, the focused ultrasound acts as a virtual light source that emits frequency-shifted photons due to acousto-optic modulation. The system selectively time-reverses the frequency-shifted photons and generates an optical focus at the position of the ultrasonic focus. As the modulation efficiency of an ultrasonic guidestar is generally below 1%, the energy gain of the system should be improved by more than two orders to compensate for the signal loss due to the ultrasound modulation. As analysed above, by simultaneously enhancing the illumination powers and applying an external electric field on the PRC, it is quite feasible to provide a two-order improvement on the energy gain of the HGHS-WFS. Accordingly, the HGHS-WFS could be extended to operation with ultrasonic guidestars.

Although we only demonstrated the HGHS-WFS at 1,064 nm, the concept can be adapted to other laser wavelengths by employing corresponding gain media (see Supplementary Note 10 for a detailed discussion).

Despite the great advantages of the HGHS-WFS, one disadvantage is that the amplified spontaneous emission (ASE) of the gain modules introduces a uniform background to the time-reversed optical focus. We employed several polarizers in our system to suppress the ASE background to a relatively low level. Considering that the spectral bandwidth of ASE is ~1 nm (Supplementary Note 11), whereas that of the signal light is narrower than 10⁻⁵ nm, the ASE background could be further suppressed through narrowband spectral filters that have subnanometre bandwidths. Such narrowband spectral filters are technically available, but highly customized designs are required⁴³. Fortunately, the ASE background is divergent and scattered further through the scattering medium. The intensity of the ASE background is therefore generally lower than that of the time-reversed focus. Furthermore, as the ASE is incoherent, the ASE background through the scattering medium is very even, which means that the time-reversed focus still has a good contrast-to-noise ratio.

Online content

Any methods, additional references, Nature Portfolio reporting summaries, source data, extended data, supplementary information, acknowledgements, peer review information; details of author contributions and competing interests; and statements of data and code availability are available at <https://doi.org/10.1038/s41566-022-01142-4>.

References

- Vellekoop, I. M. & Mosk, A. P. Focusing coherent light through opaque strongly scattering media. *Opt. Lett.* **32**, 2309–2311 (2007).
- Mosk, A. P., Lagendijk, A., Leroosey, G. & Fink, M. Controlling waves in space and time for imaging and focusing in complex media. *Nat. Photon.* **6**, 283–292 (2012).
- Wang, Y. M., Judkewitz, B., DiMarzio, C. A. & Yang, C. Deep-tissue focal fluorescence imaging with digitally time-reversed ultrasound-encoded light. *Nat. Commun.* **3**, 928 (2012).
- Akbulut, D., Huisman, T. J., van Putten, E. G., Vos, W. L. & Mosk, A. P. Focusing light through random photonic media by binary amplitude modulation. *Opt. Express* **19**, 4017–4029 (2011).
- Katz, O., Small, E., Bromberg, Y. & Silberberg, Y. Focusing and compression of ultrashort pulses through scattering media. *Nat. Photon.* **5**, 372–377 (2011).
- Conkey, D. B., Brown, A. N., Caravaca-Aguirre, A. M. & Piestun, R. Genetic algorithm optimization for focusing through turbid media in noisy environments. *Opt. Express* **20**, 4840–4849 (2012).
- Lai, P., Wang, L., Tay, J. W. & Wang, L. V. Photoacoustically guided wavefront shaping for enhanced optical focusing in scattering media. *Nat. Photon.* **9**, 126–132 (2015).
- Blochot, B., Bourdieu, L. & Gigan, S. Focusing light through dynamical samples using fast continuous wavefront optimization. *Opt. Lett.* **42**, 4994–4997 (2017).
- Frostig, H. et al. Focusing light by wavefront shaping through disorder and nonlinearity. *Optica* **4**, 1073–1079 (2017).
- Jang, M. et al. Wavefront shaping with disorder-engineered metasurfaces. *Nat. Photon.* **12**, 84–90 (2018).
- Nixon, M. et al. Real-time wavefront shaping through scattering media by all-optical feedback. *Nat. Photon.* **7**, 919–924 (2013).
- Popoff, S. M. et al. Measuring the transmission matrix in optics: an approach to the study and control of light propagation in disordered media. *Phys. Rev. Lett.* **104**, 100601 (2010).
- Kim, M. et al. Maximal energy transport through disordered media with the implementation of transmission eigenchannels. *Nat. Photon.* **6**, 581–585 (2012).
- Boniface, A., Mounaix, M., Blochet, B., Piestun, R. & Gigan, S. Transmission-matrix-based point-spread-function engineering through a complex medium. *Optica* **4**, 54–59 (2017).
- Mounaix, M., de Aguiar, H. B. & Gigan, S. Temporal recompression through a scattering medium via a broadband transmission matrix. *Optica* **4**, 1289–1292 (2017).
- Yilmaz, H., Hsu, C. W., Yamilov, A. & Cao, H. Transverse localization of transmission eigenchannels. *Nat. Photon.* **13**, 352–358 (2019).
- Mounaix, M. et al. Spatiotemporal coherent control of light through a multiple scattering medium with the multispectral transmission matrix. *Phys. Rev. Lett.* **116**, 253901 (2016).
- Conkey, D. B., Caravaca-Aguirre, A. M. & Piestun, R. High-speed scattering medium characterization with application to focusing light through turbid media. *Opt. Express* **20**, 1733–1740 (2012).
- Li, S., Horsley, S. A. R., Tyc, T., Čížmár, T. & Phillips, D. B. Memory effect assisted imaging through multimode optical fibres. *Nat. Commun.* **12**, 3751 (2021).
- Cui, M. & Yang, C. Implementation of a digital optical phase conjugation system and its application to study the robustness of turbidity suppression by phase conjugation. *Opt. Express* **18**, 3444–3455 (2010).
- Hsieh, C.-L., Pu, Y., Grange, R. & Psaltis, D. Digital phase conjugation of second harmonic radiation emitted by nanoparticles in turbid media. *Opt. Express* **18**, 12283–12290 (2010).
- Liu, Y., Ma, C., Shen, Y., Shi, J. & Wang, L. V. Focusing light inside dynamic scattering media with millisecond digital optical phase conjugation. *Optica* **4**, 280–288 (2017).
- Cheng, Z., Yang, J. & Wang, L. V. Intelligently optimized digital optical phase conjugation with particle swarm optimization. *Opt. Lett.* **45**, 431–434 (2020).
- Ruan, H. et al. Deep tissue optical focusing and optogenetic modulation with time-reversed ultrasonically encoded light. *Sci. Adv.* **3**, eaao5520 (2017).
- Ma, C., Xu, X., Liu, Y. & Wang, L. V. Time-reversed adapted-perturbation (TRAP) optical focusing onto dynamic objects inside scattering media. *Nat. Photon.* **8**, 931–936 (2014).
- Feldkhun, D., Tzang, O., Wagner, K. H. & Piestun, R. Focusing and scanning through scattering media in microseconds. *Optica* **6**, 72–75 (2019).
- Wang, D. et al. Focusing through dynamic tissue with millisecond digital optical phase conjugation. *Optica* **2**, 728–735 (2015).
- Cheng, Z. & Wang, L. V. Focusing light into scattering media with ultrasound-induced field perturbation. *Light Sci. Appl.* **10**, 159 (2021).

29. Yaqoob, Z., Psaltis, D., Feld, M. S. & Yang, C. Optical phase conjugation for turbidity suppression in biological samples. *Nat. Photon.* **2**, 110–115 (2008).
30. Xu, X., Liu, H. & Wang, L. V. Time-reversed ultrasonically encoded optical focusing into scattering media. *Nat. Photon.* **5**, 154–157 (2011).
31. Liu, Y. et al. Optical focusing deep inside dynamic scattering media with near-infrared time-reversed ultrasonically encoded (TRUE) light. *Nat. Commun.* **6**, 5904 (2015).
32. Tzang, O. et al. Wavefront shaping in complex media with a 350 kHz modulator via a 1D-to-2D transform. *Nat. Photon.* **13**, 788–793 (2019).
33. Cheng, Z., Yang, J. & Wang, L. V. Dual-polarization analog optical phase conjugation for focusing light through scattering media. *Appl. Phys. Lett.* **114**, 231104 (2019).
34. Wei, X. et al. Real-time frequency-encoded spatiotemporal focusing through scattering media using a programmable 2D ultrafine optical frequency comb. *Sci. Adv.* **6**, aay1192 (2020).
35. Hariharan, P. *Basics of Holography* (Cambridge Univ. Press, 2002).
36. Klein, M. B. Beam coupling in undoped GaAs at 1.06 μm using the photorefractive effect. *Opt. Lett.* **9**, 350–352 (1984).
37. Boyd, R. W. *Nonlinear Optics* (Academic, 2008).
38. Wang, L. V. & Wu, H. *Biomedical Optics: Principles and Imaging* (John Wiley and Sons, 2007).
39. Ruan, H., Xu, J. & Yang, C. Optical information transmission through complex scattering media with optical-channel-based intensity streaming. *Nat. Commun.* **12**, 2411 (2021).
40. Kumar, J., Albanese, G., Steier, W. H. & Ziari, M. Enhanced two-beam mixing gain in photorefractive GaAs using alternating electric fields. *Opt. Lett.* **12**, 120–122 (1987).
41. Klein, M. B., McCahon, S. W., Boggess, T. F. & Valley, G. C. High-accuracy, high-reflectivity phase conjugation at 1.06 μm by four-wave mixing in photorefractive gallium arsenide. *J. Opt. Soc. Am. B* **5**, 2467–2472 (1988).
42. Horstmeyer, R., Ruan, H. & Yang, C. Guidestar-assisted wavefront-shaping methods for focusing light into biological tissue. *Nat. Photon.* **9**, 563–571 (2015).
43. Fredell, M., Carver, G., Chanda, S., Locknar, S. & Johnson, R. *Sub-Nanometer Band Pass Coatings for LIDAR and Astronomy* 9612 (SPIE, 2015).

Publisher's note Springer Nature remains neutral with regard to jurisdictional claims in published maps and institutional affiliations.

Springer Nature or its licensor (e.g. a society or other partner) holds exclusive rights to this article under a publishing agreement with the author(s) or other rightsholder(s); author self-archiving of the accepted manuscript version of this article is solely governed by the terms of such publishing agreement and applicable law.

© The Author(s), under exclusive licence to Springer Nature Limited 2023

Methods

Experimental set-up

As shown in Fig. 2, a narrowband single-mode laser (CL1064-300-S, CrystaLaser)—with a wavelength of 1,064 nm and a linewidth of $<10^{-5}$ nm—was split into three beams through two sets of HWPs and PBSs, which were used to flexibly adjust the optical power of each beam. The two beams—reflected from the PBSs and expanded to ~4 mm diameters—constituted the reference and conjugated reference beams, and propagated through the PRC reversely and collinearly, respectively. The powers of the reference and conjugated reference beams were set to ~100 mW in all of the experiments. The probe beam (~10 mW) was transmitted through the PBSs, illuminating the scattering medium. The HWP in the path of the probe beam rotated the polarization of the probe beam to the perpendicular direction. Part of the scattered light passing through the scattering medium was collected into the two gain modules by a 50.8-mm-diameter lens. Each gain module integrated an Nd:YAG gain medium (0.8% doping concentration, 6.35 mm diameter and 140 mm length) and a pump source into a metal case, with a circulating water system for cooling. The pump source comprised several 808 nm laser diode arrays surrounding the gain medium, with a total peak pump power of 10 kW (Astrum, LT). The pulse width and the peak power of the pump output could be adjusted externally (Supplementary Note 12 shows the control flowchart of the system). The temperature of the gain crystals was set to 24 ± 0.1 °C during the experiments. We connected the two gain modules by a polarizer and a lens, which prevented half of the unpolarized ASE noise coming out of one gain module from being amplified by the other. Similarly, the polarizer in front of the first gain medium reduced the ASE noise reaching the scattering medium. Furthermore, a long-pass filter (LPF, FEL0950, Thorlabs) was used to filter the remaining pump light shorter than 950 nm in wavelength. The light out of the gain modules was condensed onto the PRC, a GaAs semiconductor with an effective area of $5 \text{ mm} \times 5 \text{ mm}$ and a thickness of 7 mm. To observe the time-reversed focus through the scattering medium directly, we inserted a beam splitter before the scattering medium to divert a copy of the time-reversed light to a camera (DCC3240N, Thorlabs). It should be noted that the plane optics around the gain modules were slightly tilted to avoid possible self-oscillation of the gain modules.

Characterizing the speckle correlation time of samples

To calibrate the relationship between the speckle correlation time and the sample movement speed, we recorded the speckle patterns on the PRC plane at different times when the sample was moving at given speeds, and calculated the correlation coefficients between the first and each of the subsequent frames of the recorded patterns. By fitting the speckle correlation coefficient versus time using a Gaussian function, we determined the correlation time of the sample at the given movement speed as the time during which the speckle correlation coefficient dropped to $1/e^2$ (e = Euler's number).

To measure the speckle correlation coefficient of a chicken tissue specimen moving at a given speed, we placed a camera capturing a region of interest of 190×190 px at a frame rate of 100 Hz in the plane of the PRC to record the speckle patterns continuously. The speckle correlation coefficient at a given time was calculated as the correlation between the speckle pattern captured at that time and the first speckle pattern. The calculated speckle correlation coefficient as a function of time t was then fitted to a Gaussian function $\alpha = A \exp(-2t/\tau_c) + B$, where A , B and τ_c are parameters to be fitted. The fitted parameter τ_c is just the correlation time of the sample. The above method works only for the measurement of correlation times larger than tens of milliseconds, limited by the frame rate of the camera recording the speckle patterns. To determine the speckle correlation time of a moving tissue specimen at a submillisecond timescale, we fitted the relationship between the measured speckle correlation time and the corresponding tissue movement speed in low-speed cases, based on

the fact that the speckle correlation time is inversely proportional to the movement speed.

To measure the speckle correlation coefficient of a living mouse's ear, we used a faster scientific complementary metal–oxide–semiconductor camera (PCO.edge, PCO AG) to record speckle patterns at a higher frame rate (2,224 fps, 160×38 px, global shutter and 0.20 ms exposure time), from which the ear's τ_c value was obtained.

Configuration details for the HGHS-WFS experiments with fast-moving tissues

In the experiments shown in Fig. 4, a piece of 4-mm-thick chicken tissue sandwiched between two glass slides was placed on a motorized translation stage (DDSM50, Thorlabs) that had a maximum movement speed of 500 mm s^{-1} and a maximum acceleration of $5,000 \text{ mm s}^{-2}$. When the motorized translation stage started to move, it sent a signal that triggered a delay generator (DG645, Stanford Research Systems). A pre-designed time delay (Δt) was set in the delay generator, and its delayed output was the ultimate signal that triggered the whole HGHS-WFS system. The delay time Δt was the time required for the motorized translation stage to accelerate to the given speed. In this way we ensured that HGHS-WFS was performed after the desired movement speed of the tissue had been reached. The starting position of the translation stage was also adjusted in each speed configuration so that the probe light illuminated the same position of the sample when the HGHS-WFS began, which could be easily determined by calculating the required acceleration distance of the motor.

In vivo animal study

We used Hsd:ATHymic Nude-Fox1^{NU} mice (Envigo)—aged ten to eleven months old—for the in vivo experiments. All experimental procedures were performed in conformity with laboratory animal protocols approved by the Institutional Animal Care and Use Committee at the California Institute of Technology. The mouse was continuously supplied with 1.5% vapourized isoflurane in air to maintain stable anaesthesia throughout the experiment. The anaesthetic state of the mouse was confirmed by pinching its hind paw. The anesthetized mouse was laid on a customized flat animal platform that also provided anaesthetic gas, and the mouse ear was sandwiched between two glass slides to act as the scattering medium. The body temperature of the mouse was maintained at 37 °C during the experiments.

Data availability

All data that support the findings of this study are available within the article and Supplementary Information, or available from the corresponding author on reasonable request.

Code availability

The codes used in this study are available from the corresponding author on reasonable request.

Acknowledgements

We appreciate J. Ballard's close reading of the paper and M. Cronin-Golomb's discussions on the photorefractive theory. This work was financially supported by US National Institutes of Health (NIH) grants R35 CA220436 (Outstanding Investigator Award) and R01 EB028277.

Author contributions

Z.C. and L.V.W. designed the study. Z.C. built the experimental system and performed the experiments. C.L. explored the amplification of scattered light at the early stage of the project. A.K. and Y.Z. prepared the living animal samples and participated in the in vivo experiments. L.V.W. supervised the project. All of the authors wrote and revised the manuscript.

Competing interests

L.W. has a financial interest in Microphotoacoustics, Inc., CalPACT, LLC, and Union Photoacoustic Technologies, Ltd., which, however, did not support this work. The other authors declare no competing interests.

Additional information

Supplementary information The online version contains supplementary material available at <https://doi.org/10.1038/s41566-022-01142-4>.

Correspondence and requests for materials should be addressed to Lihong V. Wang.

Peer review information *Nature Photonics* thanks Cheng Ma and the other, anonymous, reviewer(s) for their contribution to the peer review of this work.

Reprints and permissions information is available at www.nature.com/reprints.